

# Continuous Control of Charge Transport in Bi-Deficient BiFeO<sub>3</sub> Films Through Local Ferroelectric Switching

Tae Heon Kim, Byung Chul Jeon, Taeyoon Min, Sang Mo Yang, Daesu Lee, Yong Su Kim, Seung-Hyub Baek, Wittawat Saenrang, Chang-Beom Eom, Tae Kwon Song, Jong-Gul Yoon,\* and Tae Won Noh

It is demonstrated that electric transport in Bi-deficient Bi<sub>1- $\delta$</sub> FeO<sub>3</sub> ferroelectric thin films, which act as a p-type semiconductor, can be continuously and reversibly controlled by manipulating ferroelectric domains. Ferroelectric domain configuration is modified by applying a weak voltage stress to Pt/Bi<sub>1- $\delta$</sub> FeO<sub>3</sub>/SrRuO<sub>3</sub> thin-film capacitors. This results in diode behavior in macroscopic charge-transport properties as well as shrinkage of polarization-voltage hysteresis loops. The forward current density depends on the voltage stress time controlling the domain configuration in the Bi<sub>1- $\delta$</sub> FeO<sub>3</sub> film. Piezoresponse force microscopy shows that the density of head-to-head/tail-to-tail unpenetrating local domains created by the voltage stress is directly related to the continuous modification of the charge transport and the diode effect. The control of charge transport is discussed in conjunction with polarization-dependent interfacial barriers and charge trapping at the non-neutral domain walls of unpenetrating tail-to-tail domains. Because domain walls in Bi<sub>1- $\delta$</sub> FeO<sub>3</sub> act as local conducting paths for charge transport, the domain-wall-mediated charge transport can be extended to ferroelectric resistive nonvolatile memories and nanochannel field-effect transistors with high performances conceptually.

## 1. Introduction

The functional properties of ferroelectric materials have attracted much attention for their potential application in microelectronic devices, such as ferroelectric nonvolatile memories.<sup>[1-9]</sup> Recently, polarization control of charge transport in ferroelectrics has been extended to novel nanoelectronic devices, which include ferroelectric resistive switching memories,<sup>[10-14]</sup> ferroelectric/multiferroic tunnel junctions,<sup>[15-20]</sup> and domain wall nanoelectronics.<sup>[21-25]</sup> The modulation of interfacial potentials by electric polarization has been suggested as the origin

of ferroelectric resistive switching and switchable diode effects<sup>[6,8,26,27]</sup> that enable non-destructive readout for high-density memory applications. It has been reported that the potential profiles of the Schottky barriers for carrier injection could be selectively changed by polarization reversal.<sup>[6]</sup> This indicates that polarization charges accumulated at the interface could control the Schottky-like metal/ferroelectric interfacial barrier. The use of ferroelectric domains for continuous control of the charge transport in ferroelectric films is of further interest, because domain configuration affects polarization charge at the metal/ferroelectric interface. Such domain engineering for the control of charge transport has not been explored yet.

The robust ferroelectricity<sup>[28]</sup> and small band gap<sup>[4]</sup> of BiFeO<sub>3</sub> (BFO) are quite attractive for examining the influence of ferroelectric polarization on charge transport. At room temperature (RT), the remnant polarization ( $P_r$ ) is almost 100  $\mu\text{C cm}^{-2}$  along the [111] direction

in pseudocubic notation.<sup>[28]</sup> In addition, the band gap of BFO ( $\approx 2.2$  to 2.6 eV) is narrow compared with that of typical ferroelectric materials such as Pb(Zr,Ti)O<sub>3</sub> and BaTiO<sub>3</sub>.<sup>[4]</sup> Due to this narrow band gap, the Schottky barrier height at a metal/BFO contact can be relatively small. The large polarization charge can easily modulate interfacial barrier. These electronic characteristics make BFO as a prototype oxide semiconductor system with intriguing functionalities, such as ferroelectric resistive switching<sup>[10,12,13]</sup> and switchable photovoltaics.<sup>[4,6,9,10,27]</sup> Recently, it has been reported that the performance of resistive switching

Dr. T. H. Kim, B. C. Jeon, T. Min, S. M. Yang,  
Dr. D. Lee, Dr. Y. S. Kim, Prof. T. W. Noh  
ReCFI, Department of Physics and Astronomy  
Seoul National University  
Seoul 151-747, Korea

Dr. S.-H. Baek, W. Saenrang, Prof. C.-B. Eom  
Department of Materials Science and Engineering  
University of Wisconsin  
Madison, WI 53706, USA

Prof. T. K. Song  
School of Nano and Advanced Materials Engineering  
Changwon National University  
Changwon, Gyeongnam 641-773, Korea

Prof. J.-G. Yoon  
Department of Physics  
University of Suwon  
Hwaseong, Gyeonggi-do 445-743, Korea  
E-mail: jgyoon@suwon.ac.kr



DOI: 10.1002/adfm.201201490

devices could be improved by controlling the amount of defect charges in BFO films.<sup>[12]</sup> Even though understanding the role of defects in the controllable charge transport is a key issue in the development of high-performance electronic devices, microscopic studies of how defect charges affect the modulation of charge transport in ferroelectric films have been rare.<sup>[22–25,29]</sup>

Here, we report on continuous control of electronic transport by polarization reversal in a Bi-deficient Pt/BFO/SrRuO<sub>3</sub> (SRO) heterostructure epitaxially grown on a SrTiO<sub>3</sub> (STO)(111) substrate. To modify the domain configuration, we applied a weak voltage stress to a Bi-deficient BFO film, which acted as a p-type semiconductor, and thus controlled macroscopic charge-transport properties. Piezoresponse force microscopy (PFM) revealed that a weak voltage stress caused the nucleation and growth of reversed local domains, which did not penetrate the film thickness. The reversed local domains were responsible for the continuous modification of charge transport and diode behavior. Interestingly, we found that a weak pinning effect due to mobile defect charges could induce domain wall dragging at the pinned domain regions. We will discuss how such domain wall dragging effect could be related to charge transport as well as ferroelectric properties in Bi-deficient BFO films.

## 2. Results

For systematic investigations of charge transport, which can be affected by polarization switching and defect charges, a voltage stress experiment was designed, as shown in Figure 1a. Various electrical measurements (i.e., current density-voltage ( $J$ - $V$ ), polarization-voltage ( $P$ - $V$ ), and PFM) were separately performed for two different states: 1) pre-poled and 2) voltage-stressed. In the pre-poled state, we initially poled a BFO capacitor to have a downward polarization state by applying a 15- $\mu$ s pulse voltage of +10.0 V. After the poling process, electrical transport and ferroelectric properties were measured (marked by (1)) for a reference. To apply a voltage stress to the capacitor, we first poled the same BFO capacitor and then applied a negative dc voltage of  $V_s$ , which was smaller than the coercive voltage ( $V_c$ )  $\approx$  9 V in the pre-poled state, for a stress time of  $t_s$ . After the voltage stress process, we performed the same electrical measurements for comparison (marked by (2)). Details of thin-film fabrication and voltage stress experiments are described in the experimental section. A composition analysis of our Bi-deficient BFO(111) films is given in the Supporting Information (see Figure S1).

Figure 1b,c show changes in the  $J$ - $V$  curves and  $P$ - $V$  hysteresis loops, respectively, for different  $t_s$  with a negative voltage stress of  $V_s = -3.0$  V. As  $t_s$  increased, the  $J$ - $V$  curves became diode-like under negative bias with increasing current density. At the same time, the  $P$ - $V$  hysteresis loops were shrunk remarkably after the voltage stress with the decrease of  $P_r$  and  $V_c$ . The absolute value of  $J$  at  $V = -3.0$  V in the stressed state increased up to 2.3 mA cm<sup>-2</sup>, compared to 0.22 mA cm<sup>-2</sup> in the pre-poled state. However, the current density began to decrease again for  $t_s$  values larger than 200 s. It should be noted that a small current peak at the positive bias voltages appeared after the voltage stress. This indicated that partial polarization switching occurred during the negative voltage stress. On the other hand, hysteresis loops showed continuous decreases in  $P_r$  and  $V_c$ , from

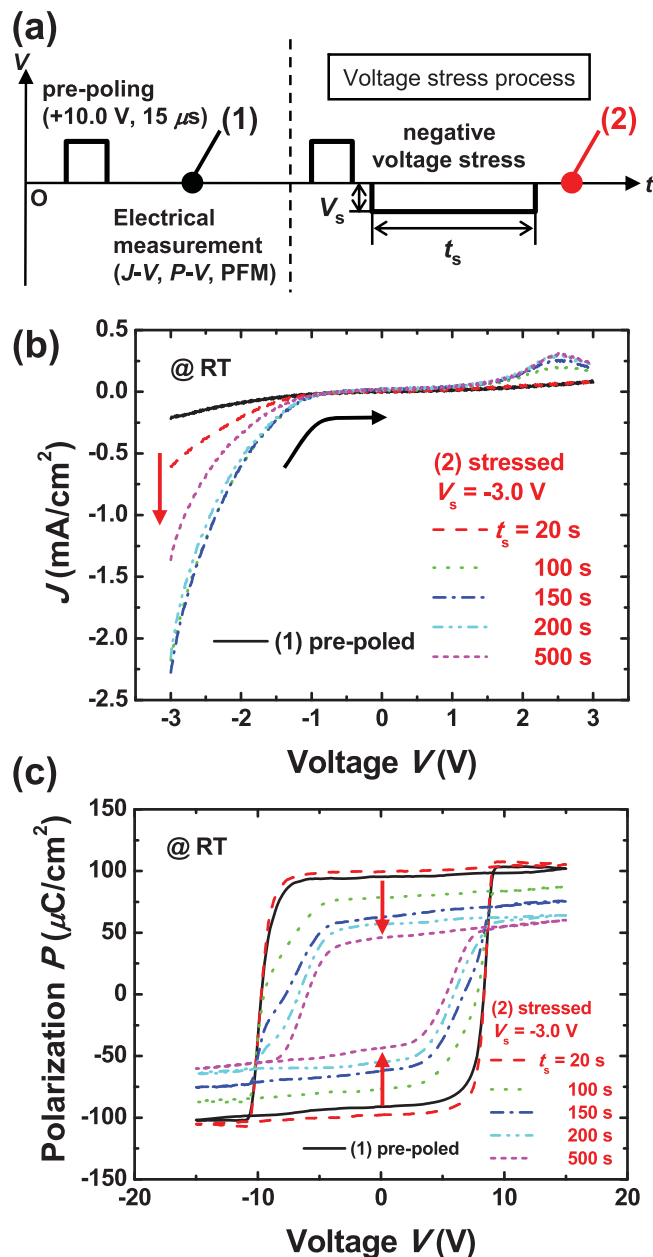


**Figure 1.** a) Electrical pulse sequences for voltage stress experiments in a Bi-deficient BFO(111) capacitor. A voltage pulse of magnitude 10.0 V and pulse width 15  $\mu$ s was applied to pre-pole a BFO(111) capacitor to downward polarization. For the pre-poled BFO capacitor, we performed electrical measurements (marked by (1)). In the voltage stress process, we applied a negative voltage stress of  $V_s$  for  $t_s$  after the initial poling process. Next, we performed the same electrical measurement for the negatively stressed BFO capacitor (marked by (2)). b)  $J$ - $V$  curves and c)  $P$ - $V$  hysteresis loops for the pre-poled and stressed states in (a). In (b), the peaks at positive voltage bias come from ferroelectric switching currents and the solid black arrow represents the sweep direction in the  $J$ - $V$  measurements. The solid red arrows in (b) and (c) represent the direction along which  $t_s$  increases.

100  $\mu$ C cm<sup>-2</sup> and 9.0 V in the pre-poled state to 47  $\mu$ C cm<sup>-2</sup> and 5.5 V in the stressed state, respectively. Apparently, the shrinkage of the hysteresis loop implied degradation of the ferroelectric

properties by the voltage stress. More interestingly, the shrunk hysteresis loops recovered to the original shape by applying a positive voltage stress (see Supporting Information Figure S2). The shrinkage and recovery of polarization hysteresis was reproducible for various voltage stresses (see Supporting Information Figure S3). This phenomena was reminiscent of the rejuvenation of ferroelectric fatigue by a high voltage stress.<sup>[1,2]</sup> For stoichiometric BFO films, these changes in  $J$ - $V$  curves and  $P$ - $V$  hysteresis loops were never observed (see Supporting Information Figure S4).

To elucidate the microscopic origin of the charge transport modification and its relation to the hysteresis loop shrinkage, we monitored the ferroelectric domain evolution during the negative voltage stress process using PFM. As shown in Figure 2a, we initially obtained PFM phase ( $\theta$ ) and amplitude ( $R$ ) images for the pre-poled state (marked by (1)). Next, we applied the half period of a 2-kHz triangular wave with the amplitude of  $-15.0$  V to switch the capacitor. Then, we imaged the corresponding domain configuration (marked by (1)<sup>sw</sup>). In the pre-poled state, the whole capacitor was switched to an upward polarization direction (bright yellow,  $\theta = 180^\circ$ ) by application of the triangular voltage pulse, as shown in Figure 2b–e. However, by referring to the  $R$  image, there seem to be randomly distributed nanodomains not penetrating the film thickness. We also performed the same PFM imaging process for the negatively-stressed states (marked by (2) and (2)<sup>sw</sup>) with different stress times ( $V_s = -3.5$  V,  $t_s = 10, 30, 40, 60,$  and  $80$  s) (Figure 2f,g). We could observe the creation and growth of upward domains clearly after application of negative voltage stress. As  $t_s$  increased, the pre-poled downward polarization (dark brown,  $\theta = 0^\circ$ ) was reversed to upward polarization (bright yellow,  $\theta = 180^\circ$ ) more and more. Considering the fact that the applied negative voltage stress was about  $V_c/3$  in the pre-poled state, the appearance of the switched domains was rather surprising. We also found that the reversed upward domains exhibited weak PFM  $R$  signals compared with the downward domains. This indicated that the nucleated upward domains did not penetrate fully across the film thickness.<sup>[30,31]</sup> These unpenetrating domains caused a decrease in the PFM  $R$  signals, because the piezoresponse was cancelled out by the opposite contributions from upward and downward domain regions. The unpenetrating domain regions could have tail-to-tail and head-to-head domain configurations across the film thickness. The local

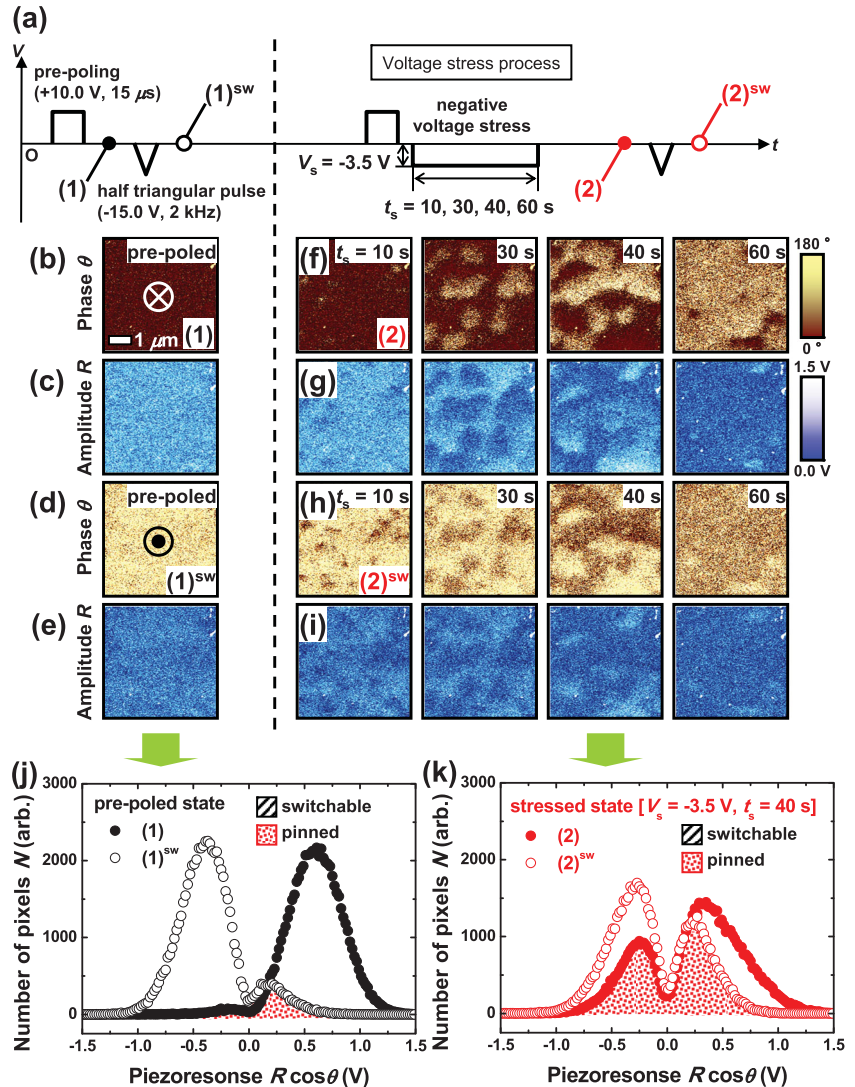


**Figure 2.** a) Electrical pulse sequences for PFM imaging of ferroelectric domains under negative voltage stress. We imaged a pre-poled state with initial downward polarization (marked by (1)). Next, by applying a half-period 2-kHz triangular pulse of amplitude  $-15.0$  V, we imaged a reversed upward polarization state (marked by (1)<sup>sw</sup>). For stressed states, we applied a constant negative voltage of  $V_s = -3.5$  V to the pre-poled BFO(111) capacitor for various  $t_s$  ( $= 10, 30, 40, 60,$  and  $80$  s) and then performed PFM imaging (marked by (2)). To examine switchable and pinned domain regions, we also applied the same half triangular pulse and imaged the ferroelectric domain configuration (marked by (2)<sup>sw</sup>). Out-of-plane PFM b,d)  $\theta$  and c,e)  $R$  images for the (1) and (1)<sup>sw</sup> states in (a). Out-of-plane PFM f,h)  $\theta$  and g,i)  $R$  images for the (2) and (2)<sup>sw</sup> states in (a). In the PFM  $\theta$  images, dark brown ( $\theta = 0^\circ$ ) and bright yellow ( $\theta = 180^\circ$ ) regions represent ferroelectric domains with downward and upward polarization, respectively. In the PFM  $R$  images, bright (large  $R$  value) and dark blue (small  $R$  value) regions represent penetrating and unpenetrating domains, respectively. The scan size of the PFM images was  $5 \times 5 \mu\text{m}^2$ . j) Distribution of  $R \cos \theta$  for the (1) and (1)<sup>sw</sup> states in (b–e). k) Distribution of  $R \cos \theta$  for the (2) and (2)<sup>sw</sup> states in (f–i). The positive and negative  $R \cos \theta$  values represent the piezoresponse of downward and upward polarization, respectively. Black hatched and red dotted regions correspond to the distributions of switchable ( $N^{\text{switchable}}$ ) and pinned domains, respectively.

switched domains should modify the Schottky barrier height at the electrode/BFO interfaces, leading to the injection of charge carriers.<sup>[6,8,26]</sup>

Analyses of the PFM images revealed that the domain walls in unpenetrating domains formed by negative voltage

stress were weakly pinned. For the pre-poled state, most of the downward domains were reversed to upward domains by a half-period triangular pulse ((1)<sup>sw</sup> in Figure 2d,e). Surprisingly, for the negatively stressed states, the unpenetrating domains with small  $R$  values looked rather backswitched even under the switching voltage pulse, whereas most of downward domains with large  $R$  values were reversed to upward domains, ((2)<sup>sw</sup> in Figure 2h,i). The apparent backswitching behavior should be interpreted as a change in the portions of upward and downward domains in the unpenetrating domain regions. This implied that the weakly pinned domain walls, which were nearly parallel to the electrodes, in the unpenetrating domains were dragged due to the interaction between trapped charges at the domain walls and the external electric field.

The weakly pinned domains suppressed the switchable polarization in our Bi-deficient BFO film. In the  $R\cos\theta$  distribution for the pre-poled state ((1) and (1)<sup>sw</sup> in Figure 2j), the positive  $R\cos\theta$  values (solid black circles) of downward polarization mostly changed to negative values (open black circles) of upward polarization (the black hatched region).<sup>[32]</sup> A small portion of pinned domains was observed, probably due to defects in our Bi-deficient BFO film (the red dotted region).<sup>[33,34]</sup> However, for the negatively stressed state, the number of pixels ( $N$ ) of switchable domains ( $N^{\text{switchable}}$ ) between (2) (solid red circles) and (2)<sup>sw</sup> (open red circles) states decreased considerably compared with that in the pre-poled state (Figure 2k; see also Supporting Information Figure S5). In contrast, the  $N$  of the pinned domains increased.

The decrease in the total volume of switchable domains due to the formation of pinned domains caused shrinkage of the polarization hysteresis loop in the Bi-deficient BFO(111) film. By summing  $N^{\text{switchable}}$  for all positive  $R\cos\theta$ , we estimated the total number of pixels of switchable domains ( $\sum_{R\cos\theta>0} N^{\text{switchable}}$ ) for both pre-poled and stressed states. As shown in Figure 3a, we found that  $\sum_{R\cos\theta>0} N^{\text{switchable}}$  was excellently in a linear relation with the  $P_r$  values in the shrunk hysteresis loops. This indicated that the pinned domains were unswitchable at a switching cycle of 2 kHz, not contributing to hysteresis loop measurement.

The enhanced diode behavior in the  $J$ - $V$  characteristics was closely related to the increase in domain wall density due to polarization switching. Ferroelectric domain walls have been known to act as local conducting paths for charge transfer.<sup>[21–25]</sup> In our Bi-deficient BFO(111) film, 180° domain walls could play the role of conduction channels.<sup>[21]</sup> Figure 3b shows that the domain wall contribution in  $R\cos\theta$  is in good agreement with the  $J(V = -3.0 \text{ V})$  values in the  $J$ - $V$  curves of Figure 1b. Note that the zero  $R\cos\theta$  in ferroelectric materials mainly comes from the piezoresponse of domain walls.<sup>[31,35,36]</sup> As  $t_s$  increased, local formation of reversed domains in stressed states increased the domain wall density and hence the current level. Compared with the current level in the pre-poled state, it was nearly an order of magnitude larger. The switched domains by a voltage stress would facilitate charge injection by lowering the Schottky-like barrier height at the interface.<sup>[6,8,26]</sup> It is highly likely that the local conduction of the injected charges through the domain walls leads to rectifying behavior in the charge transport.

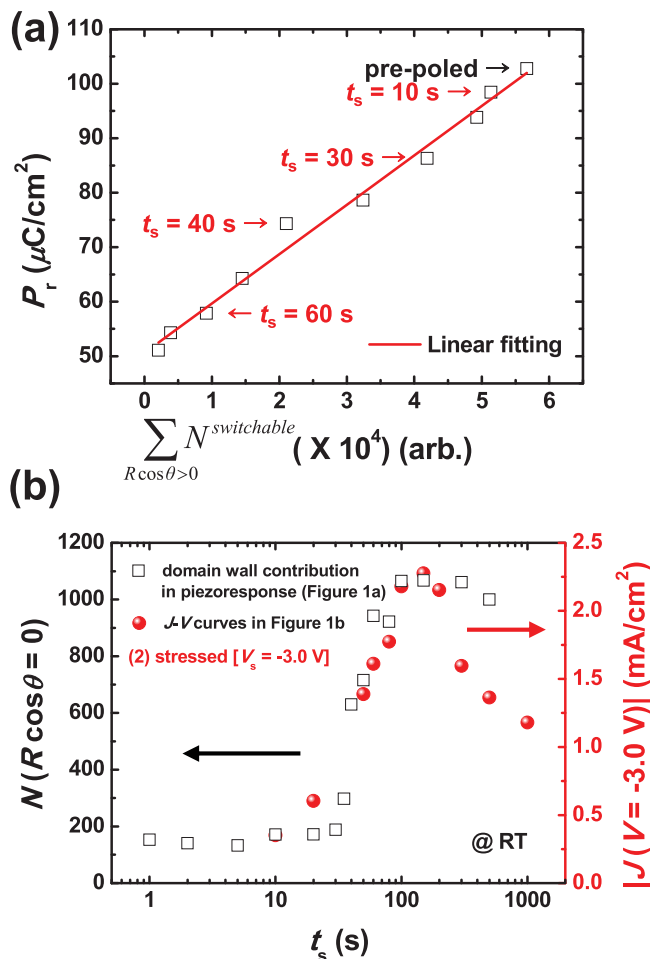


**Figure 3.** a) Correlation between  $P_r$  and  $\sum_{R\cos\theta>0} N^{\text{switchable}}$  in the pre-poled and stressed states. The red solid line represents a linear fit. b)  $t_s$ -dependent  $N(R\cos\theta=0)$  (open squares) for the stressed states ( $V_s = -3.0 \text{ V}$ ) in Figure 1a and  $|J(V = -3.0 \text{ V})|$  values (solid red circles) in the  $J$ - $V$  curves of Figure 1b. In ferroelectrics, zero  $R\cos\theta$  mainly comes from the piezoresponse of domain walls.

### 3. Discussion

Charge transport in ferroelectric films has been extensively discussed.<sup>[6,8,26]</sup> The Schottky barrier heights at ferroelectric/metal interfaces are believed to be affected by ferroelectric polarization. Lee et al. reported that switchable rectifying  $J$ - $V$  behavior in BFO capacitors arises from polarization-mediated band bending near the metal electrode/BFO interfaces.<sup>[6]</sup> Because a Bi-deficient BFO is considered to be a p-type semiconductor,<sup>[6,12,27]</sup> hole injection into the film can be facilitated by negative polarization charges bound at the interface. The continuous change in  $J$ - $V$  characteristics and shrinkage in polarization hysteresis are closely related to charge injection and trapping at the domain walls in the unpenetrating domain regions during the voltage stress.

A schematic of the domain configurations after the voltage stress is shown in Figure 4. In Figure 4a, most of the downward

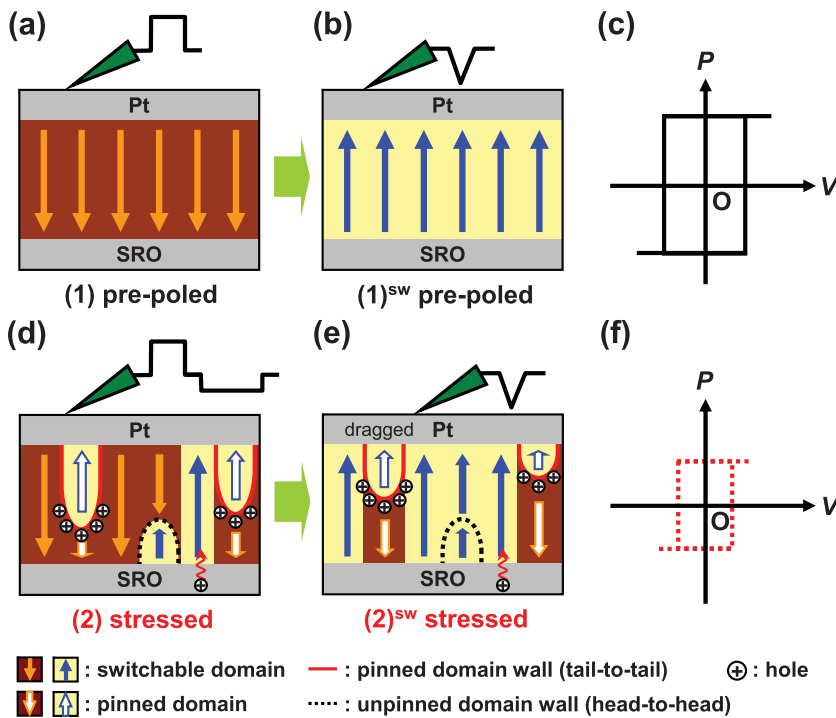


**Figure 4.** Schematic of charge-trapping-induced domain wall pinning in a Bi-deficient BFO(111) film. Ferroelectric domain configurations of a) (1) and b) (1)<sup>sw</sup> states in Figure 2a,c) the corresponding  $P$ - $V$  hysteresis loop of the pre-poled state. Ferroelectric domain configurations of d) (2) and e) (2)<sup>sw</sup> states in Figure 2a,f) the corresponding  $P$ - $V$  hysteresis loop of the pre-poled state. In (a) and (b), dark brown (bright yellow) regions with solid orange (blue) arrows represent switchable downward (upward) domains. In (d) and (e), dark brown (bright yellow) regions with open orange (blue) arrows represent pinned downward (upward) domains. In domain regions with upward polarization, holes are injected at the BFO/SRO bottom interfaces. The injected holes are trapped at tail-to-tail domain walls (red solid lines) with negative bound charges, inducing a pinning effect with the suppression of switchable polarization. In addition, the pinned domain walls are dragged due to attractive interaction between the trapped holes and negative pulse field, which causes apparent polarization backswitching in the PFM images. In contrast, head-to-head domain walls (black dotted lines) with positive bound charges are unpinning due to the absence of screening charges.

polarization in the pre-poled state is switchable. When a negative switching pulse is applied to the pre-poled BFO capacitor, the initial downward polarization is fully reversed to upward polarization, exhibiting a normal  $P$ - $V$  hysteresis loop (Figure 4b,c). However, the application of a negative voltage stress leads to partial upward polarization switching with the formation of unpenetrating nanodomains with head-to-head or tail-to-tail domain configurations, as shown in Figure 4d. Because such domain configurations induce non-charge-neutral domain walls, defect charges should be accommodated at the domain walls to screen the bound polarization charge.<sup>[23,24,29,37]</sup> Bi vacancies would be the sources of defect charges as well as lattice defects in a Bi-deficient BFO film, where holes act as dominant carriers for electronic transport.<sup>[6,12,27]</sup> At the same time, the holes can be easily injected through the SRO bottom electrode/BFO interface, of which the barrier height is locally modified by the upward polarization switching.<sup>[6,8,26]</sup> This unidirectional carrier injection in a stressed BFO capacitor induces diode behavior in the  $J$ - $V$  characteristics. The current density in the  $J$ - $V$  curves is dependent on the density of domain walls formed by the voltage stress, as mentioned above. The injected hole carriers are expected to steadily

fill trap sites formed by lattice defects.<sup>[6,10,23,29]</sup> This hole trapping will electrostatically stabilize tail-to-tail domain walls with negative bound charges, resulting in domain wall pinning (solid red lines in Figure 4d).<sup>[23]</sup> The other domain walls of the head-to-head configuration are unstable upon hole injection and thereby no pinning effect is expected in p-type BFO (dotted black lines in Figure 4d). Under a negative switching pulse, the pinned domain walls should be dragged due to the attracted holes, resulting in the apparent polarization backswitching (Figure 4e). As the pinned domains increase, the switchable polarization becomes suppressed. This causes shrinkage of the  $P$ - $V$  hysteresis loops, as shown in Figure 4f. The decrease in  $V_c$  after the voltage stress is due to the pre-existence of domains that can lower nucleation energy barrier and facilitate domain growth under low switching voltages.<sup>[32,33]</sup>

The trap-charge-induced field effect at the pinned domain walls may reduce the current flow through the conduction channel in the film, resulting in the decrease of current density in the  $J$ - $V$  curves. At the later stage of the voltage stress, i.e., for  $t_s > 200$  s, the enhanced current density decreased again (Figure 3b). Large amounts of trapped charges at the unpenetrating domain walls would produce a field effect that inhibits charge injection at the interface.<sup>[38]</sup> Our results show that local conduction with rectifying behavior in ferroelectric films could be continuously controlled using charge-trapped domain walls. Because the density of trapped charge depends on the density of unpenetrating domains, the reverse process (detrapping) is possible by applying a positive voltage stress. This corresponds to the recovery process in  $P$ - $V$  hysteresis loops, as shown in Supporting Information Figure S2. The controllable conduction properties can be used to design ferroelectric resistive switching devices with a high switching ratio.<sup>[12]</sup> Furthermore, the trap-charge-induced field effect may enable nanochannel field-effect transistors using ferroelectric nanodomains.

#### 4. Conclusion

We showed that the domain configuration manipulated by a voltage stress can be used to control charge transport in a Bi-deficient Bi<sub>1- $\delta$</sub> FeO<sub>3</sub>(111) film. Under voltage stress, switched domains penetrating the film thickness facilitate hole injection at the electrode/Bi<sub>1- $\delta$</sub> FeO<sub>3</sub> interfaces by lowering the barrier height, resulting in a diode effect. In unpenetrating domains with a tail-to-tail configuration, charge (hole) trapping occurs at domain walls. Domain pinning caused by the charge trapping results in the shrinkage of the ferroelectric hysteresis loop, which can be recovered by an opposite voltage stress. In

addition, we discussed that the trapped charges at domain walls may produce a field effect that controls charge transport through nanochannels (domain walls) in ferroelectric films. We believe that the local conduction via ferroelectric domain walls can be utilized for applications to novel nanoelectronic devices in the fields of spintronics, information storage, and communication.

## 5. Experimental Section

**Thin Film Fabrication:** Bi-deficient  $\text{Bi}_{1-\delta}\text{FeO}_3$  films were epitaxially grown on (111) STO substrates at 570 °C and 100 mTorr of oxygen via pulsed laser deposition. The Bi-deficiency in the films depended on the deposition temperature. A SRO bottom electrode was deposited at 650 °C and 100 mTorr of oxygen via pulsed laser deposition. The deposited  $\text{Bi}_{1-\delta}\text{FeO}_3(111)/\text{SRO}$  heterostructures were in situ annealed at 570 °C for 1 h after deposition under an oxygen atmosphere of 760 Torr. The epitaxy of the  $\text{Bi}_{1-\delta}\text{FeO}_3(111)$  films was confirmed through an X-ray diffraction  $\theta$ - $2\theta$  scan and a reciprocal space mapping (see Supporting Information Figure S6). No other structural phase except for the  $\text{Bi}_{1-\delta}\text{FeO}_3$  film, SRO bottom electrode, and STO substrate were observed. This indicated that the  $\text{Bi}_{1-\delta}\text{FeO}_3$  films had the same phase with pure  $\text{BiFeO}_3$  structurally. Pt top electrodes with various areas from  $10 \times 10$  to  $200 \times 200 \mu\text{m}^2$  were patterned through photolithography and sputtering. For the as-grown states, the  $\text{Bi}_{1-\delta}\text{FeO}_3(111)$  films were self-poled with downward polarization.

**dc Voltage Stress Experiments:** For voltage stress experiments, an Agilent 4155C semiconductor parameter analyzer was used. With a simple two-probe method, constant voltages of  $V_s$  were applied for  $t_s$  through the Pt top electrode. Meanwhile, the SRO bottom electrode was grounded. Before voltage stress, a BFO capacitor was pre-poled with a step pulse of magnitude 10.0 V and pulse width 15  $\mu\text{s}$ . For the voltage-stressed BFO capacitors, ferroelectric hysteresis loops were measured using the aixACCT TF analyzer 2000 by applying triangular pulses of amplitude 15 V and pulse width 2 kHz.

**Modified PFM Imaging:** To monitor ferroelectric domain evolution under dc voltage stress, a modified PFM configuration was used. The details of the modified PFM set-up were published elsewhere.<sup>[32,36]</sup> A negative voltage stress of  $V_s$  was applied to a pre-poled BFO(111) capacitor for  $t_s$ . Next, out-of-plane PFM imaging was performed under an ac bias of 0.3  $V_{\text{rms}}$  at 19.1 kHz. For each stressed state, an initial poling process was preceded.

## Supporting Information

Supporting Information is available from the Wiley Online Library or from the author.

## Acknowledgements

This work was supported by National Research Foundation of Korea (NRF) grants from the Korean government (MEST) (Grant Nos. 2009-0080567 and 2010-0020416). J.-G.Y. and T.K.S. acknowledge support from the NRF funded by MEST (Grant No. 2011-0027336). The experiments at the Pohang Light Source were supported by MEST and POSTECH. The work at University of Wisconsin-Madison was supported by the Army Research Office (ARO) under Grant No. W911NF-10-1-0362 and the National Science Foundation through grant ECCS-0708759. T.H.K. acknowledges the financial support, in part, from the Seoul Science Scholarship and Brain Korea 21.

Received: June 3, 2012

Revised: July 2, 2012

Published online:

- [1] J. F. Scott, *Ferroelectric Memories*, Springer-Verlag, Berlin **2000**.
- [2] M. Dawber, K. M. Rabe, J. F. Scott, *Rev. Mod. Phys.* **2005**, *77*, 1083.
- [3] G. Catalan, J. Seidel, R. Ramesh, J. F. Scott, *Rev. Mod. Phys.* **2012**, *84*, 119.
- [4] T. Choi, S. Lee, Y. J. Choi, V. Kiryukhin, S. W. Cheong, *Science* **2009**, *324*, 63.
- [5] S. Y. Yang, J. Seidel, S. J. Byrnes, P. Shafer, C. H. Yang, M. D. Rossell, P. Yu, Y. H. Chu, J. F. Scott, J. W. Ager, L. W. Martin, R. Ramesh, *Nat. Nanotechnol.* **2010**, *5*, 143.
- [6] D. Lee, S. H. Baek, T. H. Kim, J. G. Yoon, C. M. Folkman, C. B. Eom, T. W. Noh, *Phys. Rev. B* **2011**, *84*, 125305.
- [7] D. Lee, S. M. Yang, T. H. Kim, B. C. Jeon, Y. S. Kim, J.-G. Yoon, H. N. Lee, S. H. Baek, C. B. Eom, T. W. Noh, *Adv. Mater.* **2012**, *24*, 402.
- [8] P. W. M. Blom, R. M. Wolf, J. F. M. Cillessen, M. P. C. M. Krijn, *Phys. Rev. Lett.* **1994**, *73*, 2107.
- [9] M. Alexe, D. Hesse, *Nat. Commun.* **2011**, *2*, 256.
- [10] C. H. Yang, J. Seidel, S. Y. Kim, P. B. Rossen, P. Yu, M. Gajek, Y. H. Chu, L. W. Martin, M. B. Holcomb, Q. He, P. Maksymovych, N. Balke, S. V. Kalinin, A. P. Baddorf, S. R. Basu, M. L. Scullin, R. Ramesh, *Nat. Mater.* **2009**, *8*, 485.
- [11] J. R. Contreras, H. Kohlstedt, U. Poppe, R. Waser, C. Buchal, N. A. Pertsev, *Appl. Phys. Lett.* **2003**, *83*, 4595.
- [12] A. Tsurumaki, H. Yamada, A. Sawa, *Adv. Funct. Mater.* **2012**, *22*, 1040.
- [13] A. Q. Jiang, C. Wang, K. J. Jin, X. B. Liu, J. F. Scott, C. S. Hwang, T. A. Tang, H. B. Lu, G. Z. Yang, *Adv. Mater.* **2011**, *23*, 1277.
- [14] D. Pantel, S. Goetze, D. Hesse, M. Alexe, *ACS Nano* **2011**, *5*, 6032.
- [15] E. Y. Tsymbal, H. Kohlstedt, *Science* **2006**, *313*, 181.
- [16] V. Garcia, S. Fusil, K. Bouzehouane, S. Enouz-Vedrenne, N. D. Mathur, A. Barthelemy, M. Bibes, *Nature* **2009**, *460*, 81.
- [17] M. Y. Zhuravlev, R. F. Sabirianov, S. S. Jaswal, E. Y. Tsymbal, *Phys. Rev. Lett.* **2005**, *94*, 246802.
- [18] P. Maksymovych, S. Jesse, P. Yu, R. Ramesh, A. P. Baddorf, S. V. Kalinin, *Science* **2009**, *324*, 1421.
- [19] A. Gruverman, D. Wu, H. Lu, Y. Wang, H. W. Jang, C. M. Folkman, M. Y. Zhuravlev, D. Felker, M. Rzchowski, C. B. Eom, E. Y. Tsymbal, *Nano Lett.* **2009**, *9*, 3539.
- [20] D. Pantel, S. Goetze, D. Hesse, M. Alexe, *Nat. Mater.* **2012**, *11*, 289.
- [21] J. Seidel, L. W. Martin, Q. He, Q. Zhan, Y. H. Chu, A. Rother, M. E. Hawkrige, P. Maksymovych, P. Yu, M. Gajek, N. Balke, S. V. Kalinin, S. Gemming, F. Wang, G. Catalan, J. F. Scott, N. A. Spaldin, J. Orenstein, R. Ramesh, *Nat. Mater.* **2009**, *8*, 229.
- [22] N. Balke, B. Winchester, W. Ren, Y. H. Chu, A. N. Morozovska, E. A. Eliseev, M. Huijben, R. K. Vasudevan, P. Maksymovych, J. Britson, S. Jesse, I. Kornev, R. Ramesh, L. Bellaiche, L. Q. Chen, S. V. Kalinin, *Nat. Phys.* **2011**, *8*, 81.
- [23] D. Meier, J. Seidel, A. Cano, K. Delaney, Y. Kumagai, M. Mostovoy, N. A. Spaldin, R. Ramesh, M. Fiebig, *Nat. Mater.* **2012**, *11*, 284.
- [24] S. Farokhipoor, B. Noheda, *Phys. Rev. Lett.* **2011**, *107*, 127601.
- [25] J. Guyonnet, I. Gaponenko, S. Gariglio, P. Paruch, *Adv. Mater.* **2011**, *23*, 5377.
- [26] L. Pintilie, M. Alexe, *J. Appl. Phys.* **2005**, *98*, 124103.
- [27] S. Y. Yang, L. W. Martin, S. J. Byrnes, T. E. Conry, S. R. Basu, D. Paran, L. Reichertz, J. Ihlefeld, C. Adamo, A. Melville, Y. H. Chu, C. H. Yang, J. L. Musfeldt, D. G. Schlom, J. W. Ager, Iii, R. Ramesh, *Appl. Phys. Lett.* **2009**, *95*, 062909.
- [28] J. Wang, J. B. Neaton, H. Zheng, V. Nagarajan, S. B. Ogale, B. Liu, D. Viehland, V. Vaithyanathan, D. G. Schlom, U. V. Waghmare, N. A. Spaldin, K. M. Rabe, M. Wuttig, R. Ramesh, *Science* **2003**, *299*, 1719.
- [29] J. Seidel, P. Maksymovych, Y. Batra, A. Katan, S. Y. Yang, Q. He, A. P. Baddorf, S. V. Kalinin, C. H. Yang, J. C. Yang, Y. H. Chu, E. K. H. Salje, H. Wormeester, M. Salmeron, R. Ramesh, *Phys. Rev. Lett.* **2010**, *105*, 197603.

- [30] S. M. Yang, T. H. Kim, J.-G. Yoon, T. W. Noh, *Adv. Funct. Mater.* **2012**, 22, 2310.
- [31] S. Hong, E. L. Colla, E. Kim, D. V. Taylor, A. K. Tagantsev, P. Muralt, K. No, N. Setter, *J. Appl. Phys.* **1999**, 86, 607.
- [32] D. J. Kim, J. Y. Jo, T. H. Kim, S. M. Yang, B. Chen, Y. S. Kim, T. W. Noh, *Appl. Phys. Lett.* **2007**, 91, 132903.
- [33] S. Jesse, B. J. Rodriguez, S. Choudhury, A. P. Baddorf, I. Vrejoiu, D. Hesse, M. Alexe, E. A. Eliseev, A. N. Morozovska, J. Zhang, L.-Q. Chen, S. V. Kalinin, *Nat. Mater.* **2008**, 7, 209.
- [34] J. Y. Jo, S. M. Yang, T. H. Kim, H. N. Lee, J. G. Yoon, S. Park, Y. Jo, M. H. Jung, T. W. Noh, *Phys. Rev. Lett.* **2009**, 102, 045701.
- [35] A. Gruverman, D. Wu, J. F. Scott, *Phys. Rev. Lett.* **2008**, 100, 097601.
- [36] S. M. Yang, J. Y. Jo, D. J. Kim, H. Sung, T. W. Noh, H. N. Lee, J. G. Yoon, T. K. Song, *Appl. Phys. Lett.* **2008**, 92, 252901.
- [37] S.-H. Baek, C. M. Folkman, J.-W. Park, S. Lee, C.-W. Bark, T. Tybell, C.-B. Eom, *Adv. Mater.* **2011**, 23, 1621.
- [38] S. M. Sze, K. K. Ng, *Physics of Semiconductor Devices*, Wiley, Hoboken **2007**.
-